NPS69-82-002

NAVAL POSTGRADUATE SCHOOL
Monterey, California

DTIC
SELECTED
JUL 2 2 1982
F

WIND-TUNNEL DRAG MEASUREMENTS OF A

BALL-OBTURATED TUBULAR PROJECTILE

R. H. Nunn
W. A. Bry

June, 1982

Approved for public release; distribution unlimited.

Naval Weapons Center
China Lake, Ca 93555

82 07 22 065

NAVAL POSTGRADUATE SCHOOL
Monterey, California

J. J. Ekelund, RADM, USN   D. A. Schrady
Superintendent   Acting Provost

This report was prepared by:

ROBERT H. NUNN
Professor
Department of Mechanical Engineering

Reviewed by: Released by:

P. J. Marto, Chairman   William M. Tolles
Department of Mechanical   Dean of Research
    Engineering

REPORT DOCUMENTATION PAGE		READ INSTRUCTIONS BEFORE COMPLETING FORM
1. REPORT NUMBER NPS69-82-002	2. GOVT ACCESSION NO. AD-A117368	3. RECIPIENT'S CATALOG NUMBER
4. TITLE (and Subtitle) WIND-TUNNEL DRAG MEASUREMENTS OF A BALL-OBTURATED TUBULAR PROJECTILE		5. TYPE OF REPORT & PERIOD COVERED Final Report
		6. PERFORMING ORG. REPORT NUMBER
7. AUTHOR(s) R. H. Nunn W. A. Bry		8. CONTRACT OR GRANT NUMBER(s)
9. PERFORMING ORGANIZATION NAME AND ADDRESS Naval Postgraduate School Monterey, California 93940		10. PROGRAM ELEMENT, PROJECT, TASK AREA & WORK UNIT NUMBERS 62332N; F32300000 N60530 81WR30044
11. CONTROLLING OFFICE NAME AND ADDRESS Technology Programs Management Office (Code 3205) Naval Weapons Center China Lake, CA 93555		12. REPORT DATE June, 1982
		13. NUMBER OF PAGES 30
14. MONITORING AGENCY NAME & ADDRESS(if different from Controlling Office)		15. SECURITY CLASS. (of this report) UNCLASSIFIED
		15a. DECLASSIFICATION, DOWNGRADING SCHEDULE

16. DISTRIBUTION STATEMENT (of this Report)

Approved for public release; distribution unlimited

17. DISTRIBUTION STATEMENT (of the abstract entered in Block 20, if different from Report)

18. SUPPLEMENTARY NOTES

19. KEY WORDS (Continue on reverse side if necessary and identify by block number)

Aerodynamics, Tubular projectile, Base drag

20. ABSTRACT (Continue on reverse side if necessary and identify by block number)

Drag measurements and Schlieren flow visualizations have been obtained for a prototype ball-obturated tubular projectile. The test range included Mach numbers of 1.94, 2.88, and 4.00 and a full range of obturator positions was surveyed at each Mach number.

The results indicate that with the ball partially open the projectile internal flow field is severely complicated by combined viscous and shock wave interactions. A large part of the drag reduction due to ball opening

iii

is obtained during the final motion of the ball and the partially open con-
dition may lead to drags above those of the standard projectile, particularly
at the lower Mach numbers.

With the ball closed, the projectile configuration is dominated by
bluff-body drag and the drag on the ball itself may be estimated by the
previously espoused theory.

Accession For

NTIS GRA&I   X
DTIC TAB
Unannounced
Justification

By
Distribution/
Availability Codes

Dist | Avail and/or
     | Special

A

DTIC
COPY
INSPECTED

SUMMARY

Drag measurements and Schlieren flow visualizations have been obtained for a prototype ball-obturated tubular projectile. The test range included Mach numbers of 1.94, 2.88, and 4.00 and a full range of obturator positions was surveyed at each Mach number.

The results indicate that with the ball partially open the projectile internal flow field is severely complicated by combined viscous and shock wave interactions. A large part of the drag reduction due to ball opening is obtained during the final motion of the ball and the partially open condition may lead to drags above those of the standard projectile, particularly at the lower Mach numbers.

With the ball closed, the projectile configuration is dominated by bluff-body drag and the drag on the ball itself may be estimated by the previously espoused one-dimensional theory.

INTRODUCTION

Ball obturation of a tubular projectile provides an automatic and relatively simple means by which a tubular projectile may be launched without the disadvantages associated with plugs, sabots, and other more-conventional obturation methods. Figure 1 illustrates one of the earlier designs of a ball-obturated projectile developed at the Naval Weapons Center (NWC) [1] and it is this configuration that has been the subject of theoretical and experimental investigations at the Naval Postgraduate School (NPS).

Reference [2] reports the content and capabilities of an analytical model developed to describe the motion of the obturating ball within the spinning tubular projectile. Chief among the necessary inputs to this model is a formulation of the aerodynamic forces acting upon the ball during its motion from a blocking position to one in which flow through the projectile is unobstructed. In order to establish the nature and level of these forces, an experimental program has been conducted at NPS to measure the projectile drag as a function of ball position and flight Mach number. These tests are fully described in [3] and this report summarizes the major results of the tests as well as the implications of the results upon the motion of the obturating ball.
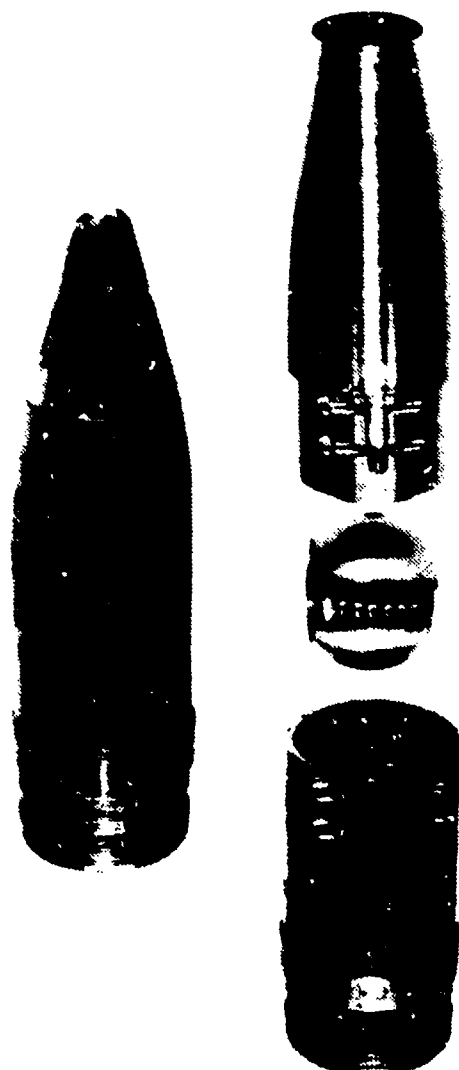
Figure 1. Conventional 20-mm and ball-obturated tubular projectiles modified for wind-tunnel testing.

EXPERIMENTAL APPARATUS

WIND TUNNEL

The wind tunnel used for all testing is pictured in Fig. 2 and a view of the test section is provided in Fig. 3. The wind tunnel is of a fixed Mach number blowdown type with a nominal test-section cross-sectional area of 0.1 m square. Interchangeable nozzle blocks were used to allow tests at nominal Mach numbers of 1.94, 2.88, and 4.00. (Although the transient behavior of the projectile flow field during continuous Mach number variations is of particular interest, an investigation of this aspect of BOP performance must await the availability of a more sophisticated wind-tunnel facility.)

In addition to the usual necessary control and supply instrumentation, the wind tunnel was equipped with plenum and test-section static pressure measurements for the determination of test-section Mach number to within an estimated maximum uncertainty of $\pm$ 2.2%. The determination of this and other experimental uncertainties, as well as a detailed description of the experimental apparatus, are described in [3].

STRAIN-GAGE BALANCE

Design of the balance constituted a major portion of the study. A variety of mechanical and electrical means for sensing pressure and force were considered. Design requirements for the balance were as follows:

1. Strength sufficient to handle drag forces estimated to be as high as 30N with adequate provision for transient peaks and design uncertainties.

2. Structural support for the projectile in the tunnel was to be obtained with a minimum of interference and flow obstruction.
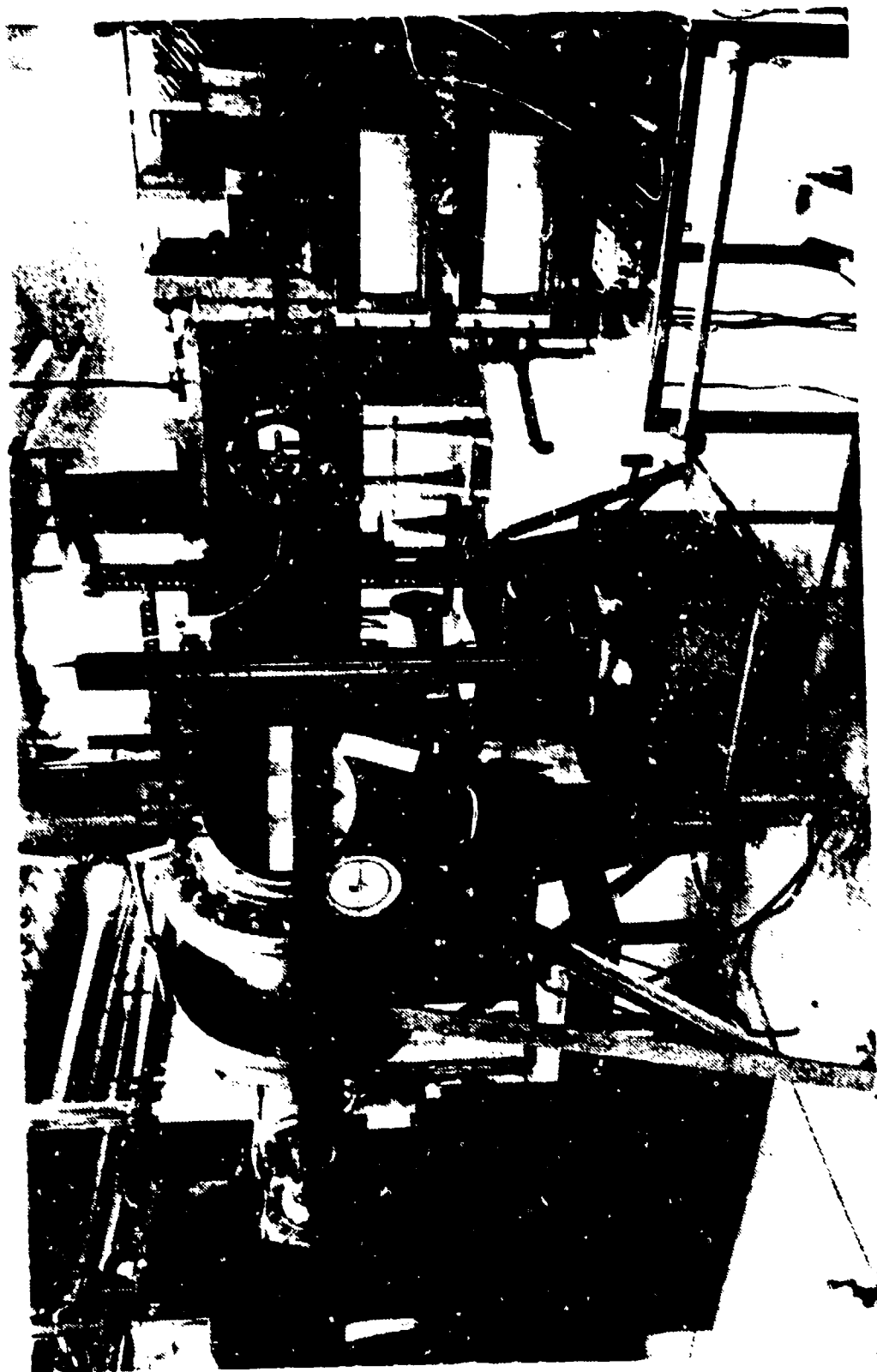
3

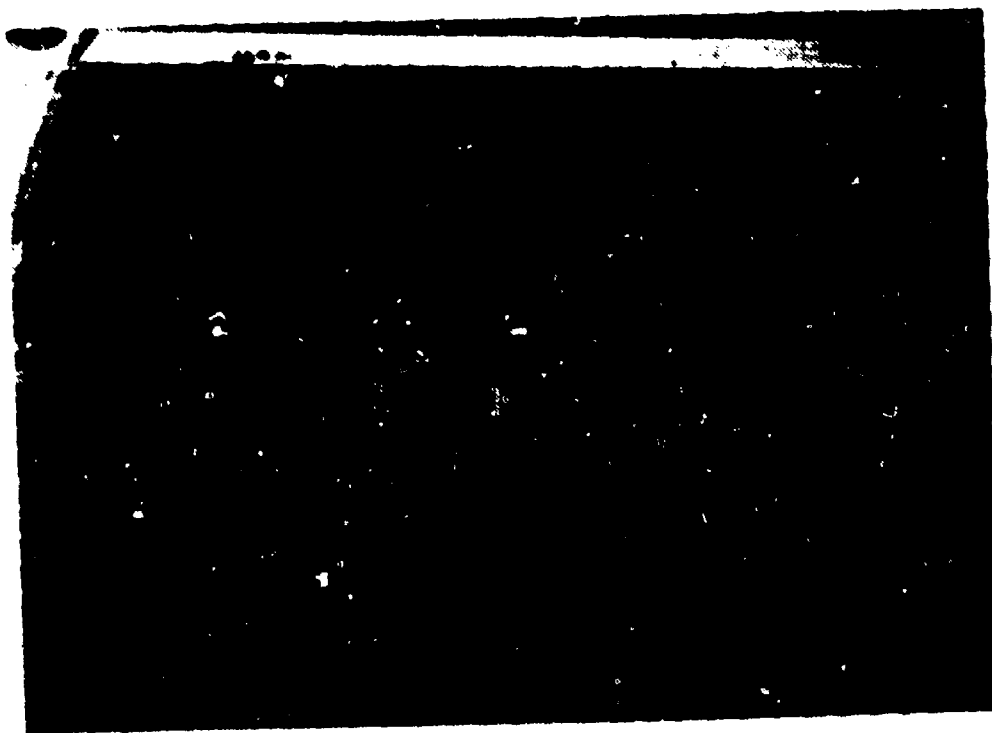Figure 2. Wind tunnel and associated experimental apparatus

3

Figure 3.   M56 projectile mounted in the wind-
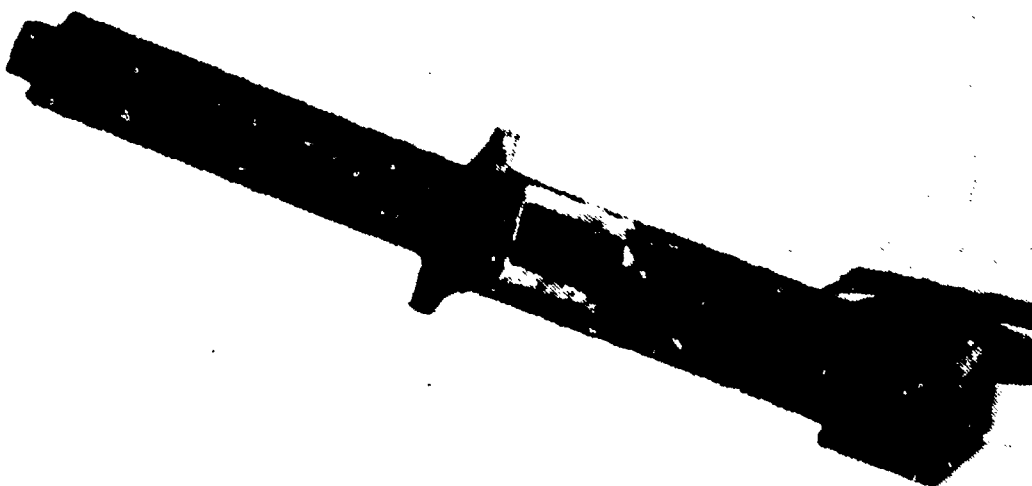tunnel on initial balance design.

Figure 4.   Final balance design.

5

3. An unobstructed view through the side ports was necessary to make the Schlieren photographs.

4. The nozzle block design allowed instrumentation to be inserted through the lower wall only; it was made of a workable phenolic while the upper block was solid steel.

5. The balance instrumentation had to be insensitive to environmental temperature, pressure and humidity changes.

6. The balance itself had to be sturdy enough to withstand possibly severe vibrations caused by turbulent shear and tunnel start-up transients.

7. Allowance was needed to provide for quick adjustments to the test projectile through the removable viewing ports.

8. The projectile support strut had to provide the smallest aerodynamic interference possible so its contribution to the total measured quantities was minimized.

9. The strain gage arrangement was to provide maximum sensitivity to aerodynamic forces while being of minimum size and relatively insensitive to spurious signals.

A number of design iterations (one of which is shown in Fig. 3) were necessary to satisfy these requirements. The final balance design is shown in Fig. 4 and in the design drawing of Fig. 5. The single strut was designed for minimum drag by maximizing the width dimension, (16.5 mm), and keeping it as thin as possible, (3.8 mm). The mount was also designed to maximize the distance, ℓ, from ball center to strut center. The longer this moment arm could be made the higher would be the moments experienced at the point of measurement. A further advantage of the new design was that the

Figure 5.   Final   balance design-sketch.
All dimensions in millimeters.

7

single wedge-shaped strut lent itself to interference drag approximations by using standard compressible flow theory.

Strain gages were mounted on the balance cantilever using standard techniques. Originally, each of four gages was wired to a separate recording channel and to an identical temperature compensating gage. The compensators were mounted as close as physically possible below the cantilever part of the balance. Temperature compensation proved inadequate with this gage configuration, however, because of the extreme sensitivity of the gages and the rapid temperature changes that occurred during tunnel start-up. Because of these difficulties it eventually became necessary to depart from a design using four independent gages, each with a separate temperature compensation gage, and to operate with two independent gage sets (A-B and C-D in Fig. 5) with each set mutually compensating. Temperature compensation was thus achieved with a doubling of the balance signal-to-noise ratio but with the loss of an ability to measure lift forces.

INTERFERENCE DRAG DETERMINATIONS

The final major problem encountered in the testing procedure was that of estimating what part of the total measured drag and moment was caused by the projectile alone. Deviations of the total measured quantities from those due to the projectile alone were assumed to result from balance, tunnel, and projectile interactions and will be referred to as tare quantities. The interactions included form and frictional drag on exposed balance parts, flows through small gaps between baseplate and tunnel floor, shock waves formed on the baseplate leading edge and unknown pressure gradients across the test section.

8

Several methods were considered to estimate these "tare" quantities, and it was finally decided to use a standard M56 20-mm projectile for which the drag had been measured in actual firing tests [4]. The drag of the standard projectile $(C_{D_{TS}})$ was measured at each test Mach number and the difference between this drag and the reported drag of the projectile alone $(C_{D_{PR}})$ was taken as an indication of the tare drag $(C_{D_{TA}})$ associated with the characteristics of the wind-tunnel and mounting configurations. In addition to this more-or-less direct determination, the drag $(C_{D_{TH}})$ on the wedge-shaped strut was estimated using inviscid theory and provided a "feel" for the extent to which the strut contributed to the total interference effect. The results of these estimates are given below in Table I.

Table I. Drag Coefficient Correction Comparison

M_∞	$C_{D_{TS}}$	$C_{D_{PR}}$*	$C_{D_{TA}}$	$C_{D_{TH}}$
1.94	.820	.465	.355	.288
2.88	.648	.388	.260	.183
4.0	.476	.316	.160	.136

*The reference drag coefficient for M = 4.0 was obtained through private communication with the Naval Weapons Center, China Lake, CA, Code 3247. Values at other Mach numbers are those reported in [4].

TUBULAR PROJECTILE WIND-TUNNEL MODEL

The tubular projectile was modified so that the ball was restricted to rotation about its pitch axis only. It could be pinned in nine different rotation angles, Θ, by use of a set screw and dimples machined into the ball. The finished product is shown in Fig. 1 along with the standard 20-mm projectile. Fig. 5 includes a cross sectional drawing of the modification.

RESULTS

Figures 6, 7, 8, and 9 show C_D as a function of Θ. The ball is full open at $\Theta = 0$ and full closed for values of Θ greater than 75 degrees. The uncertainty band calculations were performed as recommended by Ref. [5], and were based on results for the ball angle giving the most-scattered data for each Mach number. Table II gives numerical values for the maximum fractional uncertainty associated with the major experimental parameters.

Table II. Drag Coefficient Uncertainty (worst case)

M_∞	$\dfrac{\Delta M_\infty}{M_\infty}$	$\dfrac{\Delta D}{D}$	$\dfrac{\Delta C_D}{C_D}$
1.94	.022	.099	.126
2.88	.014	.155	.169
4.0	3.55 E-5	.04	.05

Although the dependency of the drag coefficient upon ball angle is generally in accordance with expectations (rising as the ball closes) it is interesting to note that the drag rise is relatively gradual and essentially complete well before the opening through the projectile is completely blocked. This may be attributed to the combined effects of viscosity and shock wave interaction within the projectile when the ball is in a partially-open position. Thus, the flow is effectively blocked even though the ball is partially open (within a range of $50^0 < \Theta < 60^0$, say).

Further support of this conclusion is provided by the series of Schlieren photographs taken at each ball position and Mach number (Figs. 10-12) in which the emergence of the bow shock wave is seen to begin at relatively low ball angles. The bow-shock behavior is in itself an interesting phenomenon and is
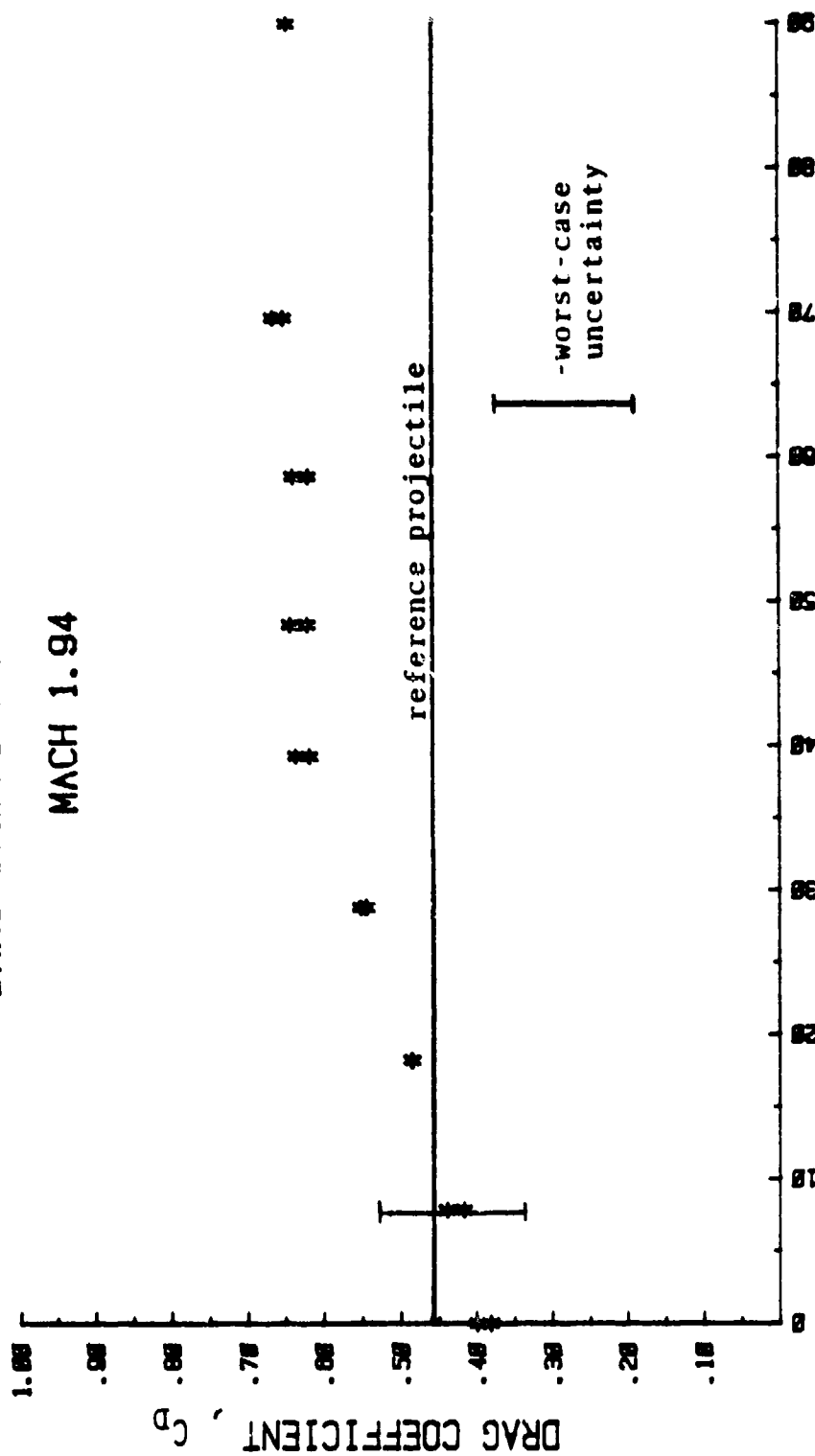
Figure 6. Drag Coefficient vs. Ball Angle. $M_\infty = 1.94$.

11
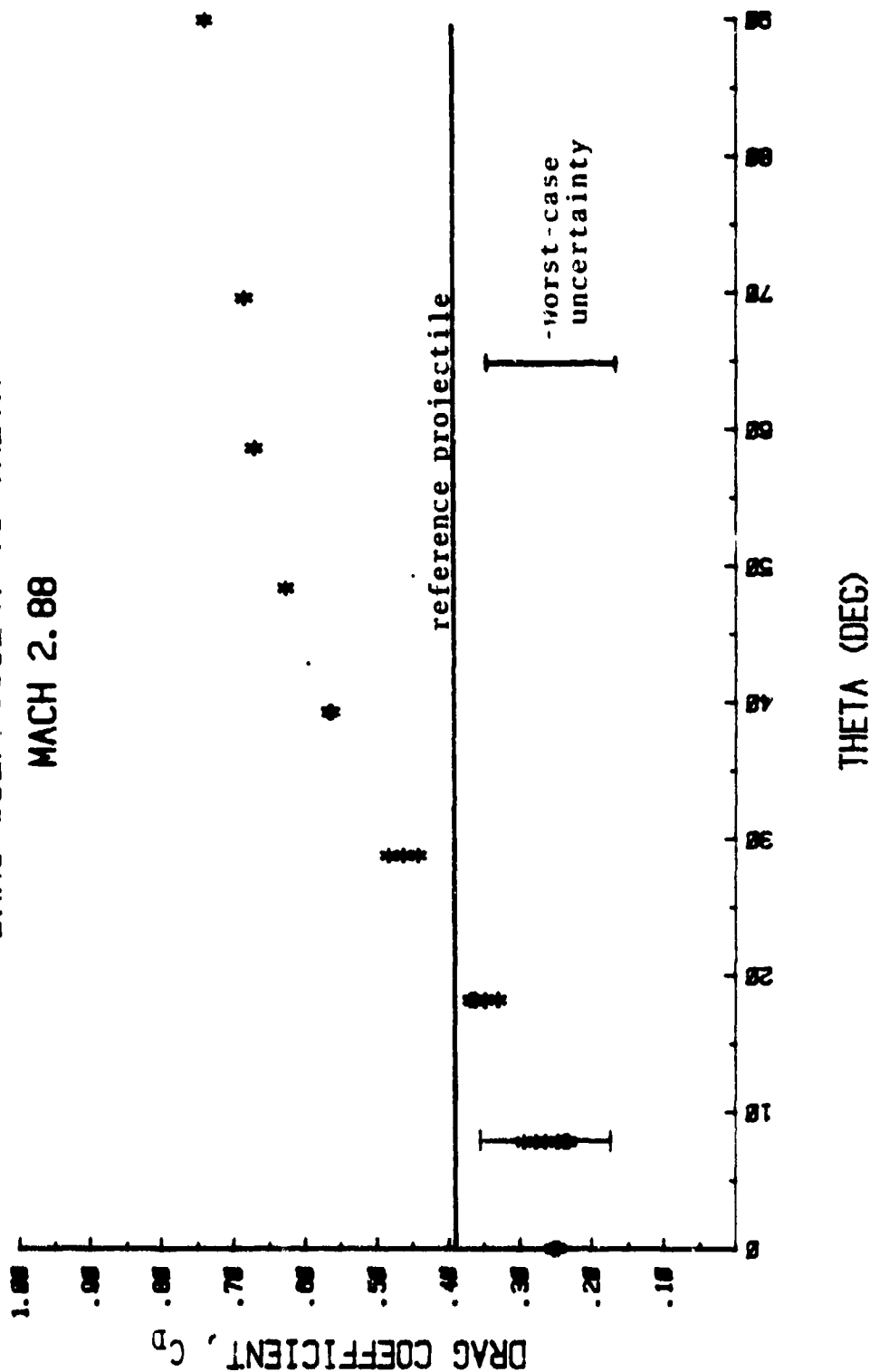
Figure 7. Drag Coefficient vs. Ball Angle. $M_\alpha = 2.88$.

Figure 8. Drag Coefficient vs. Ball Angle. $M_\infty = 4.0$.

13
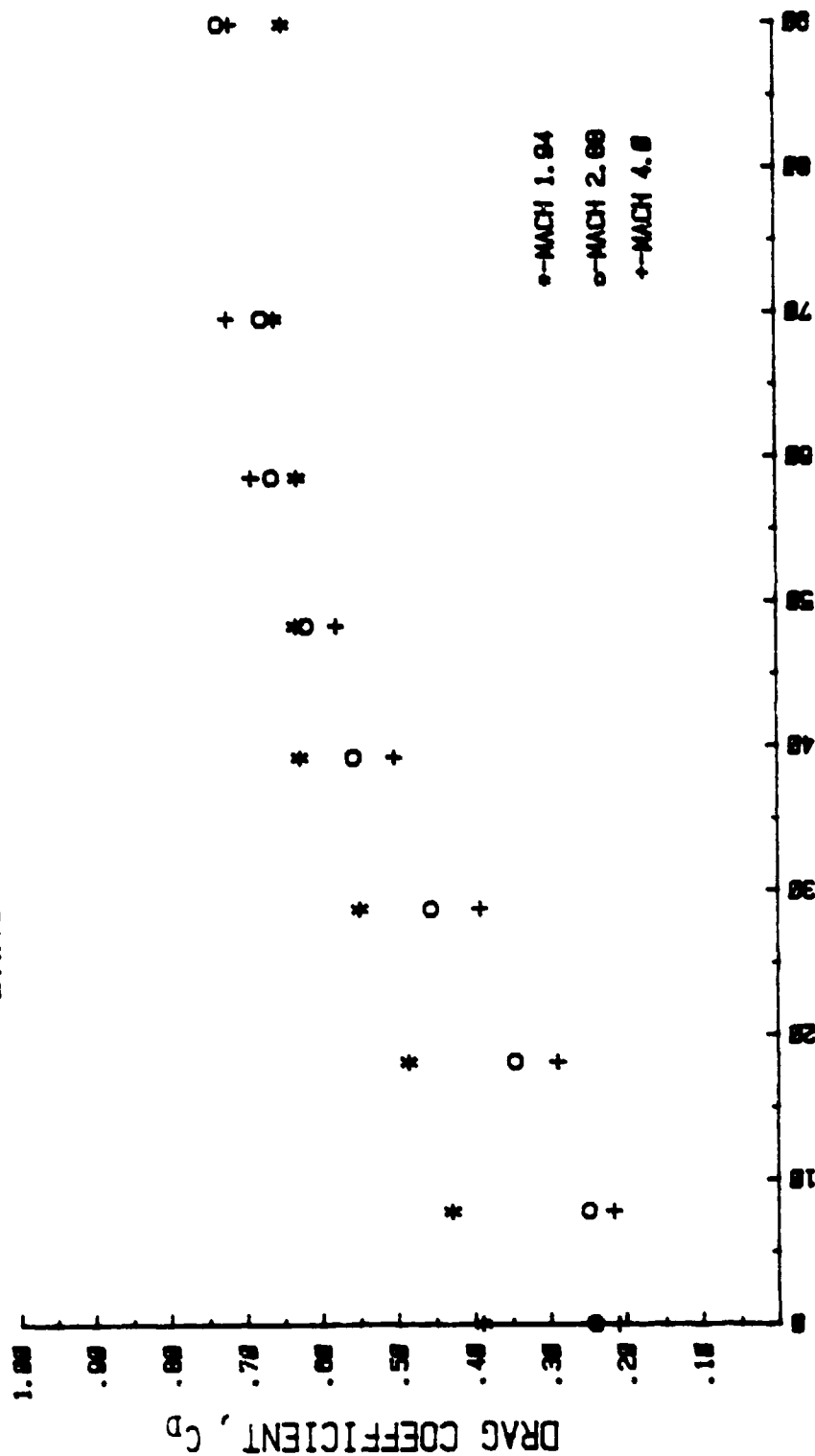
Figure 9. Mean Drag Coefficients vs. Ball Angle, Combined.

14

shown in Figs. 10-12 to exhibit gradual dependency upon ball angle rather than the sudden appearance dictated by simple one-dimensional compressible flow theory. The Schlieren photographs indicate that shock swallowing is a gradual process as the ball opens (Θ decreases) with more opening (a larger critical flow area) required at the lower Mach numbers. At a Mach number of 1.94, for instance, the ball must be aligned with the projectile axis to within less than 18.2° for the shock to be swallowed. The corresponding angle at Mach 4.0 is about 40°.

In any case, the bow-shock swallowing process is gradual and the benefits accruing from drag reduction due to projectile flow-through occur over a range of ball angles. Interestingly, the point where the drag curves change from a distinct positive slope to an asymptotic behavior occurs somewhat after initial bow shock detachment. This is well after the point where supersonic flow is no longer expected within the projectile.

Figure 9 shows that the Mach 1.94 curve crosses the other two at about $\Theta = 50$ degrees. As the ball closes (to higher angles) the Mach 1.94 drag coefficient remains the lowest of the three. This may be explained by the fact that with the ball fully closed the projectile behaves essentially as a blunt object. Without the advantages of a streamlined projectile the drag increases as the pressure rise across the bow shock increases with Mach number. Therefore, the blunt body wave drag becomes the predominant part of the total drag for the higher ball angles.

The same reasoning may be used to explain why a greater drag reduction is indicated for the full open ball position at Mach 4.0 than at the lower Mach numbers. The conventional M56 round has a somewhat blunt shaped nosecone. In a small region near the apex of that cone the pressure distribution may be
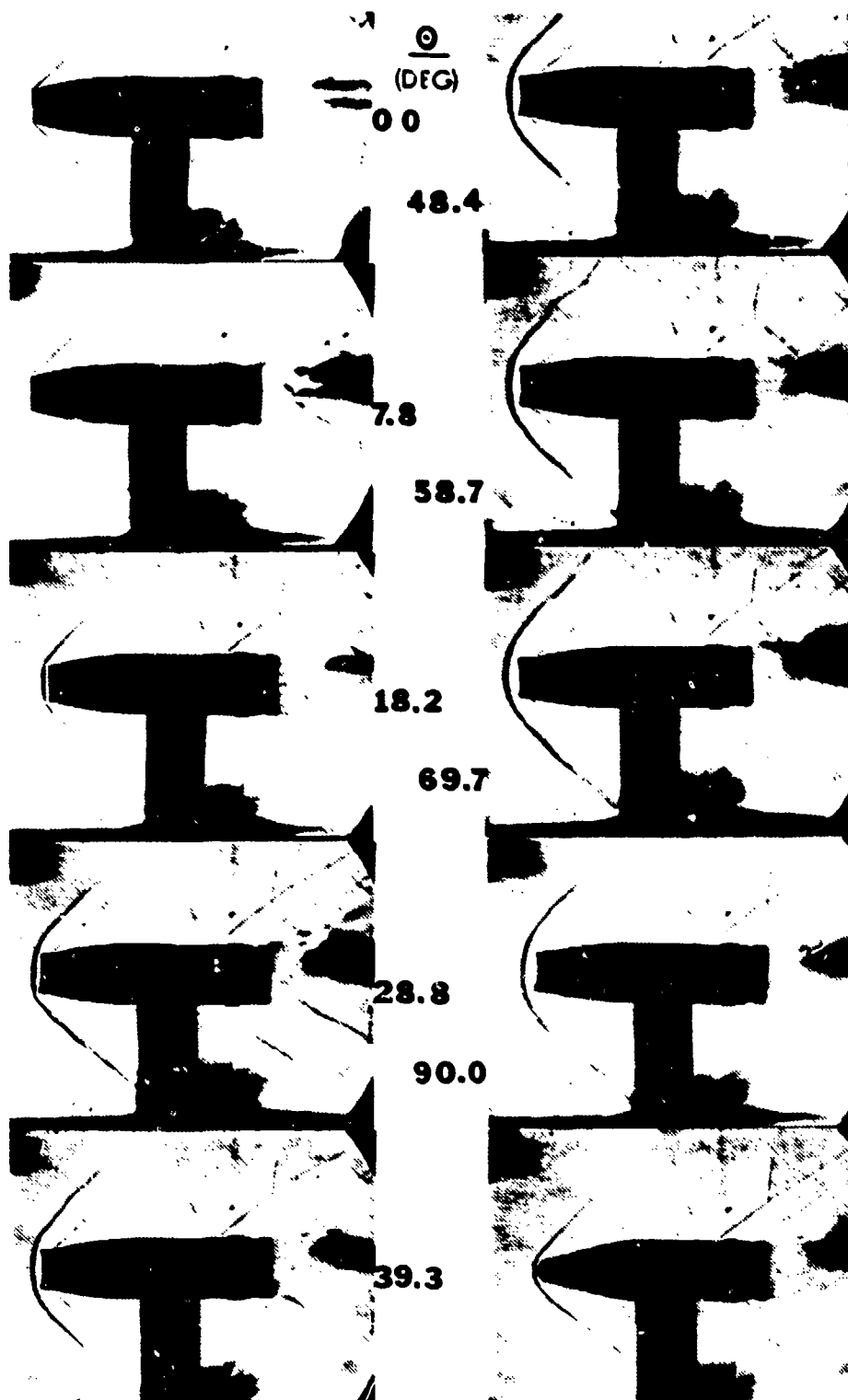
15

Figure 10. Schlieren series - Mach 1.94.

16

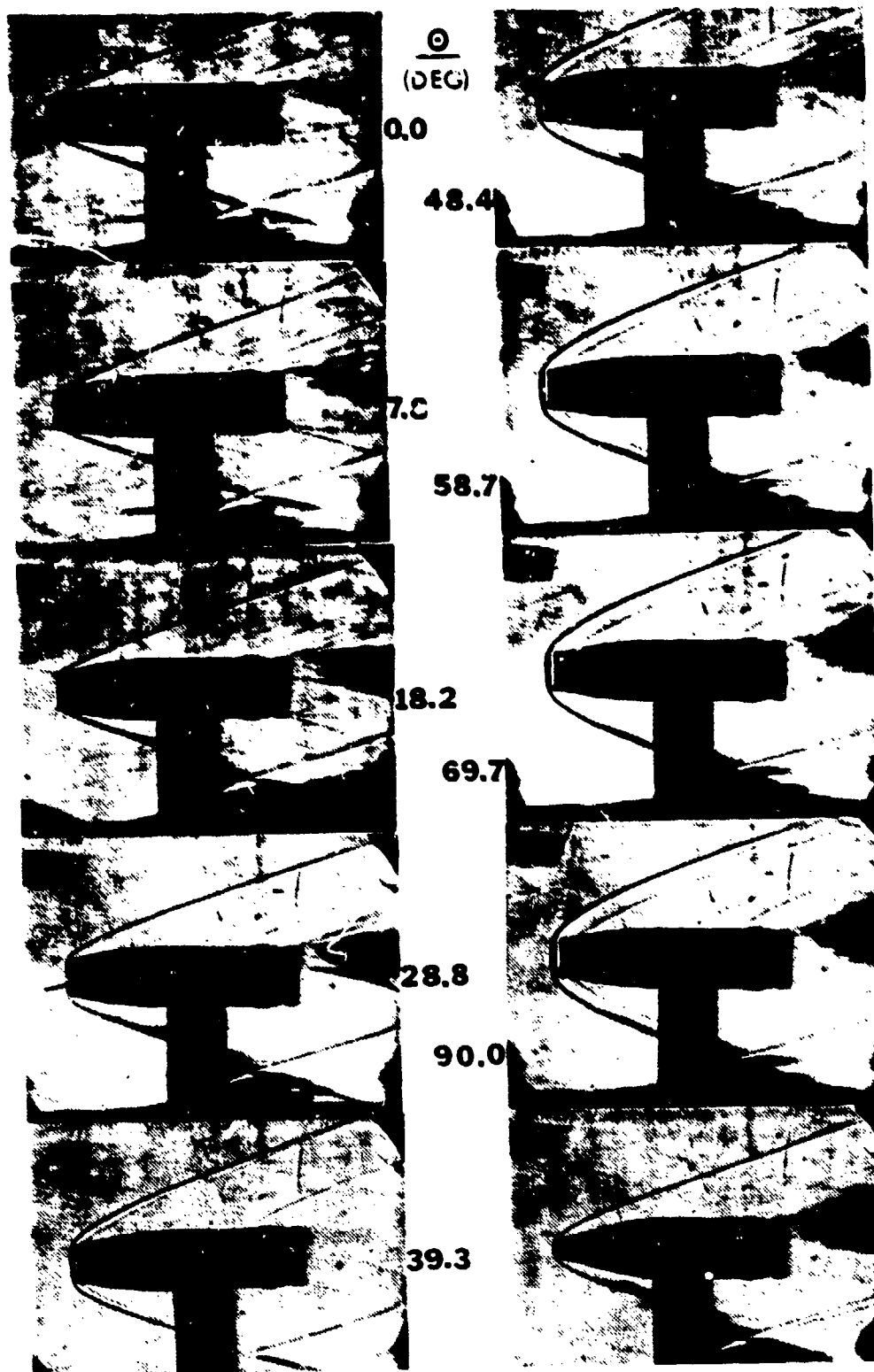Figure 11. Schlieren series - Mach 2.88.

Figure 12. Schlieren series - Mach 4.0.

approximated by blunt-body behavior; that is, the ratio of pressures across the shock is about equal to the ratio across a normal shock. The ratio of pressures across a normal shock is 4 times higher at Mach 4 than at Mach 2. Therefore, when this region is removed, as it is in a tubular projectile, the drag reduction will be greater at the higher Mach numbers.

IMPLICATIONS REGARDING BALL MOTION

As has been mentioned, a major purpose of these tests was to obtain an estimate of the forces acting upon the ball within the projectile. The drag component of these forces may be deduced from the drag data for the entire projectile under the hypothesis that the drag force on the ball is negligible with the ball entirely open. Thus, if C_{D_0} is the value of C_D at $\Theta = 0$, then the ball drag C_{D_B} may be estimated as

$$C_{D_B} = C_D - C_{D_0}$$

or

$$\frac{C_{D_B}}{C_{D_{BC}}} = \frac{C_D - C_{D_0}}{C_{D_C} - C_{D_0}}$$

where $C_{D_{BC}}$ and C_{D_C} are the ball and projectile drag coefficients, respectively, with the ball closed. (The interpretation of the data in this fashion requires the neglect of the unknown variation of interference drag with ball position.) With the data of Figs. 6-9 (see [3] for the raw data), Fig. 13 has been prepared to illustrate the ball drag as a function of ball angle. The ball-open and ball-closed drag coefficients are given for the three Mach numbers in Table III.

The scatter in the data of Fig. 13 is seen to be particularly severe at the low Mach number and at ball angles near the closed position. This is largely attributable to the experimental difficulties encountered at the lower Mach numbers and is not sufficient to disguise the doubly-asymptotic behavior of the data. It appears that the data in this form might be amenable to correlative schemes aimed at producing an empirical expression for the ball

drag as a function of ball angle and Mach number. (This effort has not been undertaken.) Note that from Fig. 13 it may be deducted that approximately 75% of the total drag reduction available occurs at ball angles less than 45° (half-open).

Table III. Ball Open ($\Theta = 0$) and Ball Closed ($\Theta = 90^O$) Drag Coefficients

	M_∞		
	1.94	2.88	4.00
Projectile			
Ball Open, C_{D_0}	0.390	0.250	0.210
Ball Closed, C_{D_C}	0.645	0.738	0.714
Ball $C_{D_{BC}} = C_{D_C} - C_{D_0}$	0.255	0.488	0.504
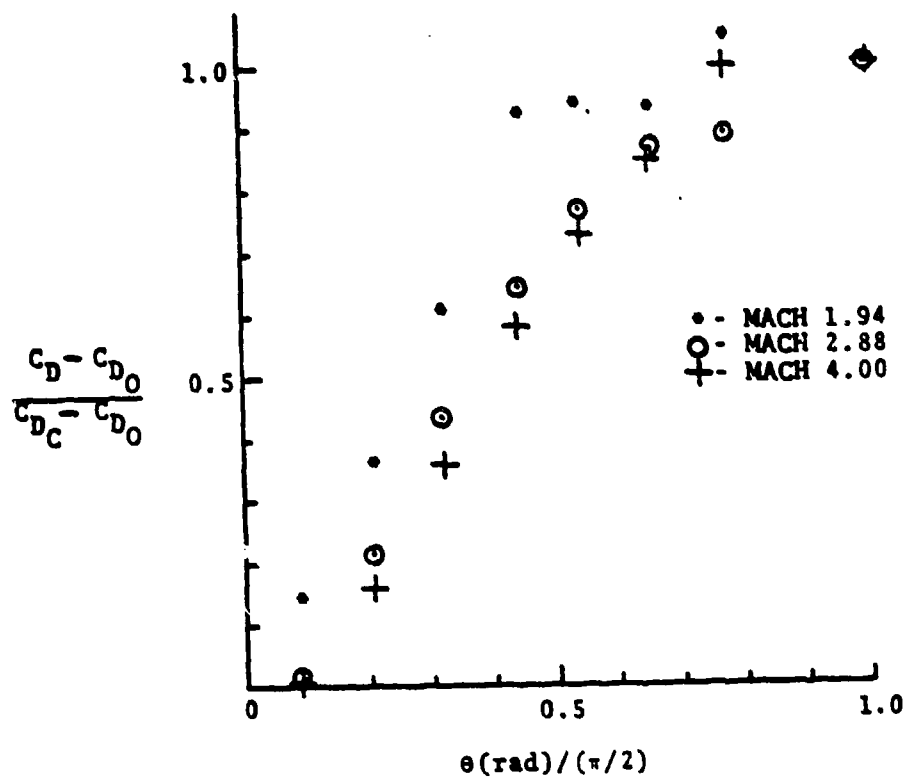
Figure 13. Ball drag coefficient vs ball angle.

21

Of particular interest in the analysis developed in [2] is the aerodynamic drag on the ball in the closed position. This force is primary in determining the dynamic behavior of the ball and in [2] it was approximated assuming freestream static pressure on the face of the ball and negligible base pressure recovery. Under these assumptions, the ball drag coefficient is given as:

$$C_{D_{BC}} = 4\bar{r}^2 (1 - 1/M_{\infty}^2) / (k + 1)$$

where $\bar{r}$ is the ratio of ball hole radius to the projectile radius and k is the isentropic exponent. Using the parameters pertinent to these experiments ($\bar{r} = 0.573$ and $k = 1.4$) the drag coefficient for the fully-closed ball is given theoretically as:

$$C_{D_{BC}} = 0.55 (1 - 1/M_{\infty}^2)$$

This expression is compared with the experimental values (Table III) in Fig. 14.
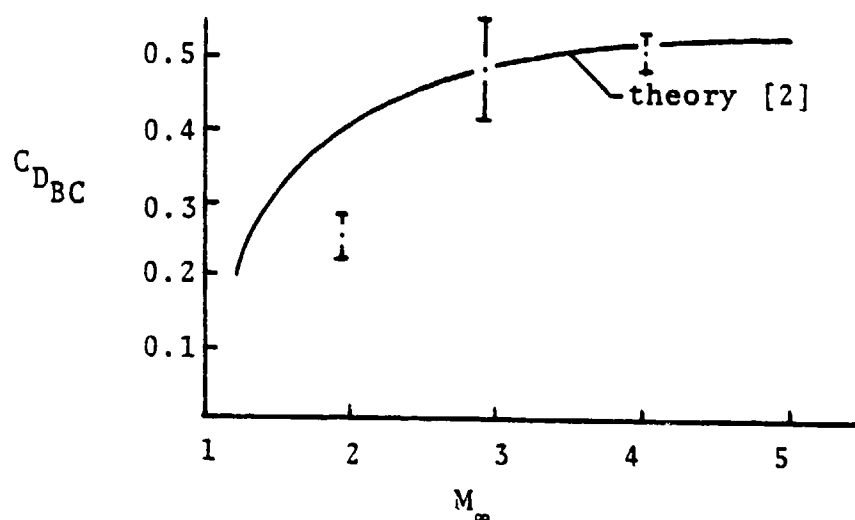

Figure 14. Drag coefficient of closed ball. Comparison with theory.

Given the experimental uncertainties (the error bands shown in Fig. 14 represent the most extreme case), the formula recommended in [2] appears to be well-supported by the data. The departure of theory from experiment at low Mach numbers is not unexpected since the theoretical prediction is sensitive to differences between normal-shock downstream static and stagnation pressures. These differences become insignificant at the higher Mach numbers.

LIST OF REFERENCES

1. Black, W., "Ball Actuated Tubular Projectile," patent disclosure, Navy Case No. 63902, 1978.

2. Naval Postgraduate Report 69-81-001, Ball Motion in a Ball-Obturated Tubular Projectile, by R. H. Nunn and J. W. Bloomer II, January, 1981.

3. Bry, W. A., Aerodynamic Loads on a Ball-Obturated Tubular Projectile, Masters Thesis, Naval Postgraduate School, Monterey, CA, March, 1982.

4. Ballistic Research Laboratories Memorandum Report No. 2192, Comparative Evaluation of the 20-mm Developmental Ammunition-Exterior Ballistics, by Maynard J. Piddington, Aberdeen Proving Ground, Maryland.

5. Holman, J. P., Experimental Methods for Engineers, Third Edition, McGraw-Hill Book Company, 1978.

DISTRIBUTION